Crystallization kinetics of sol-gel derived hydroxyapatite thin films

C. M. LOPATIN[1]*, V. B. PIZZICONI[2], T. L. ALFORD[3]
[1]Department of Chemical and Materials Engineering, Arizona State University, Tempe, AZ 85287–6006
[2]Department of Bioengineering, Arizona State University, Tempe, AZ 85287–9709
[3]Department of Chemical and Materials Engineering, Arizona State University, Tempe, AZ 85287–6006
E-mail: vincent.pizziconi@asu.edu

The crystallization kinetics of sol-gel derived hydroxyapatite (HA) and tricalcium phosphate (TCP) thin films were studied to determine whether viscous sintering could be used for densification. The films were approximately 900 nm thick, and were synthesized and processed on silicon substrates. The films were fired in air in a rapid thermal annealer (RTA) for various times and the degree of crystallinity was determined by measuring the intensity of characteristic X-ray diffraction lines. The growth kinetics of HA and TCP were measured between 420 and 550 °C, and between 840 and 920 °C, respectively. Films that were subjected to an accelerated aging step before firing, exhibited a significantly lower crystallization growth rate when compared to unaged films. The aged films also became harder, as measured by nanoindentation. At temperatures above 840 °C, HA transformed into both α- and β-TCP, with the β form being dominant at lower temperatures. The activation energies for both transformations (amorphous film to HA, and HA to TCP) were determined, as were the constants for the Avrami equation. Based on the rapid crystallization kinetics observed for the amorphous film to HA transformation, densification through viscous sintering is essentially precluded in this system.

1. Introduction

The bioceramic hydroxyapatite ($Ca_{10}[PO_4]_6[OH]_2$, HA) is frequently used to coat titanium medical implants to improve tissue fixation and thus increase the lifetime of the implant [1]. While the plasma spray method is most commonly used to coat metallic implants [2], this method has been associated with adhesive failure [1] and also has the general problem in that it is difficult to modify the microstructure of the coating to achieve optimum response in the body. The sol-gel method is an alternative means to form coatings, and has several advantages [3]. First, the microstructure of solids obtained using sol-gel techniques can be modified by changing the chemistry and/or processing conditions. In addition, submicron thin films of uniform thickness can be made using sol-gel techniques. Such thin films are amenable to ion-beam modification techniques, which can be used to increase film adhesion and density [4, 5].

Ceramics formed using sol-gel techniques are initially not fully dense, and further densification is typically performed by high temperature viscous sintering [6]. In general however, the presence of a crystalline structure impedes the sintering process by precluding viscous flow [7]. For this reason, it is desirable to maintain the amorphous structure until densification is complete, and then induce crystallization to the desired phase. To facilitate such a procedure, time-temperature-transformation (*T-T-T*) curves have been used to find the optimum processing path [8].

In this context, the main goal of this study was to obtain the transformation kinetics of the amorphous gel to crystalline HA in thin films and thus determine whether high temperature sintering is a viable densification route in this system. In addition, a recurring goal was to determine the factors controlling HA crystallization in sol-gel systems.

Previous work on this sol-gel system [9] has shown that crystalline HA films and powders can be formed at temperatures exceeding 400 °C. The current study examines the early stages of HA thin film crystallization over the temperature range of 420–460 °C. It is anticipated that much higher temperatures will be necessary to achieve full HA density, and thus the (expected) transformation from HA to tricalcium phosphate at temperatures above 840 °C was also examined. The kinetic information obtained consists of the activation

*Present address: National Research Council Post-Doctoral Associate, NASA Langley Research Center, Hampton, VA 23681.

energies, frequency factors and representation of the various transformations in the form of *T-T-T* diagrams.

2. Experimental

The sol precursor was made using *n*-butyl acid phosphate (*n*-BAP) and calcium nitrate tetrahydrate as the phosphorous and calcium sources, respectively. The reactions were performed at room temperature in a solvent of 2-methoxyethanol at a molar concentration of 0.15. The quantities of the calcium and phosphorus sources were set to maintain a ratio of 1.667. Since calcium and phosphorus are non-volatile at the processing temperatures used here, this ratio is maintained throughout the film synthesis. This result has been confirmed in several studies of the stoichiometry of the final films [10, 11]. Details of the procedure can be found elsewhere [10].

The sol was deposited on a silicon wafer and spun at a rate of 3000 rpm for 10 s, forming films approximately 900 nm thick. After spinning the film was immediately dried at 300 °C for 5 min, driving off any residual solvent. As typically found using this procedure, the dried films had a mirror finish and the color was uniform across the film, indicating uniform thickness. The thickness of the films was determined using a Dektak II stylus profilometer to measure the height of a step incorporated into the film. After drying, the samples were fired in air using a rapid thermal annealer (RTA). The heating rate was 10 °C/s, except where noted.

Isothermal tests were performed at temperatures ranging from 420 to 460 °C for the gel to HA study, and from 840 to 920 °C for the HA to TCP study. The time increments used in the isothermal tests ranged from 7 to 300 s. After each time increment the degree of crystallinity was determined by measuring the intensity of a strong X-ray diffraction line characteristic of the phase under study [12]. Preliminary tests indicated that, over the temperature range studied, three phases were present: HA and α- and β-TCP. For the gel to HA transformation study the HA (2 1 1) diffraction line was used, while for the HA to β-TCP study the (0 2 10) line of β-TCP was used [the decrease in intensity of the HA (2 1 1) line was observed in this transformation, but not used for the analysis].

A total of four sets of experiments were performed. In the first series of experiments the transformation of the film from an amorphous gel to crystalline HA was studied. In the second series of experiments an accelerated aging cycle was introduced, consisting of holding the samples at 350 °C (significantly below the temperature at which HA is formed) for 3 min before performing the isothermal tests. The third series of tests were performed to determine the kinetics of the HA to β-TCP transformation. In this series, each sample was first fired at 750 °C for 3 min to form a highly crystalline HA structure, and then fired isothermally at higher temperatures to start the transformation. In the fourth series of experiments the kinetics of the HA to TCP transformation was determined for films which did not undergo the initial HA crystallization step. In this test series, the films were heated at the much higher rate of 100 °C/s to the desired holding temperature to avoid the lower temperature, HA formation regime. In this series of experiments the effect of the finite cooling time was to introduce a limited amount of HA into the sample after the isothermal hold; and therefore a new, unfired sample was used to obtain data for each time increment. Thus, each isothermal growth curve derived from these experiments consists of data from separate samples. The experimental conditions for all the experiments described above are summarized in Table I.

X-ray diffraction analysis was performed using a Philips MRD diffractometer with Cu K_α radiation and a graphite monochrometer. At first, both glancing angle and θ–2θ scans were performed. It was found that while equivalent diffraction peaks were present in the two types of scan, the diffraction lines from the glancing angle scans were much more distinct, as would be expected for thin films. The data reported here were thus obtained in glancing angle mode, using a glancing angle of 3°. The value of 2θ was incremented in steps of 0.01°/s. Nanoindentation was used to determine the hardness of the films. A Hysitron nano-indentor was used, with a Berkovich tip. The loading rate was 20 micro-newtons/s.

3. Results

3.1. Amorphous gel to crystalline hydroxyapatite transformation

The X-ray spectra for a film that had not been fired, a film fired at 750 °C for 3 min, and the JCPDS HA standard [13] are shown in Fig. 1. It can be seen that the unfired sample shows no evidence of crystallinity. In addition, there is no evidence of the broad line at $2\theta = 32°$ characteristic of amorphous calcium phosphate, $Ca_3(PO_4)_2 \cdot 3\text{-}4.5H_2O$ (ACP) [14]. Also, all the diffraction lines appearing in the fired sample corresponded to the HA standard, indicating that no secondary crystalline

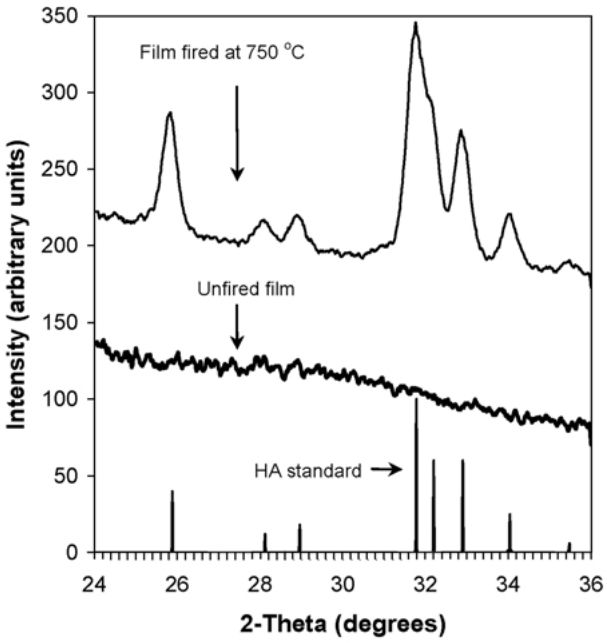

Figure 1 X-ray diffraction pattern of an unfired film and a film fired in air at 750 °C for 3 min. Both films were dried at 300 °C for 5 min. Also shown is the JCPDS HA powder standard [13]. No evidence of any crystalline material is found in the unfired film, and all the diffraction lines in the fired film correspond to HA. $\lambda = 0.15406$ nm.

TABLE I Experimental test conditions

Test series	Initial phase	Final phase	Temperature range	Heating rate
1	Amorphous gel	Hydroxyapatite	420–460 °C	10 °C/s
2	Amorphous gel-aged	Hydroxyapatite	420–460 °C	10 °C/s
3	Hydroxyapatite	α- and β-TCP	840–920 °C	10 °C/s
4	Amorphous gel	α- and β-TCP	860–900 °C	100 °C/s

phases were present. Fig. 1 demonstrates that tri-calcium phosphate (TCP) did not form below 750 °C.

Figs 2 and 3 show the results corresponding to the isothermal growth experiments on unaged and aged samples, respectively. These figures were constructed as follows. The intensity of the HA (2 1 1) peak recorded at the end of each series of isothermal runs was normalized to 1. This normalized intensity value corresponds to diffraction from fully crystallized material, and thus was used to compare the intensity values of samples fired for shorter times. Each data point thus corresponds to the intensity of the (2 1 1) line, at that time and temperature, divided by the maximum observed intensity of the (2 1 1) line. The error bars shown represent the difference between two isothermal tests performed under identical conditions.

The Avrami equation, shown below, was used to model the isothermal growth data [15, 16]:

$$X = 1 - \exp(-\kappa t^n)$$

where X is the fraction of material transformed from the amorphous gel to crystalline HA, t is the firing time, and κ and n are fitting constants. The values of n and κ were determined by rewriting the Avrami equation as $\ln(-\ln(1-X)) = \ln(\kappa) - n\ln(t)$, and performing a least squares fit to the isothermal growth data. The values of κ and n determined for each curve are tabulated in Table II. The large r values (correlation coefficient) of the fits indicate that the isothermal growth curves are well described by the Avrami equation.

The activation energy E_a, representing the growth of the crystalline phase, was determined using the following procedure [17]. A particular value for the fraction transformed was chosen for each isothermal growth curve, in this case a value of 0.8 was chosen. While any value could have been chosen, using 0.8 takes advantage of the fact that the different isothermal curves are most separated at this value (see Figs 2 and 3), and thus the method described below for finding the activation energy is more accurate. The Avrami equation, for $X = 0.8$, can thus be rewritten as $\kappa t_{0.8}^n = \text{constant}$, where $t_{0.8}$ is the time required to transform 0.8 of the gel to crystalline HA. This can be rewritten as $\ln\kappa + n\ln(t_{0.8}) = \text{constant}$. It is usually assumed that κ will follow Arrhenius behavior, $\kappa = \kappa_0 \exp(E_a/kT)$, where E_a corresponds to the combined activation energies of nucleation and growth, k = Boltzman's constant. Thus $E_a/kT + n\ln(t_{0.8}) = \text{constant}$. The activation energy corresponding to the transformation can thus be found by plotting $\ln(t_{0.8})$ versus $1/T$ and finding the slope. Fig. 4 shows the results of this procedure for the unaged and aged samples. It is evident the transformation follows Arrhenius behavior. It can also be seen that the activation energy is higher in the aged compared to the un-aged samples, indicating that aging raises the energy barrier, thus hindering transformation. This result is also reflected in the time-temperature-transformation curves discussed below. The computed values for the activation energies for the un-aged and aged samples are 189 and 231 kJ/mol, respectively (1.96 and 2.39 eV/mol). The

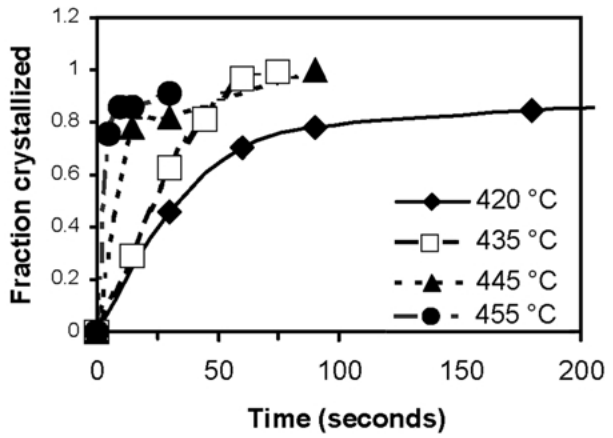

Figure 2 Isothermal growth curves corresponding to the transformation from the amorphous film to crystalline HA in unaged films. The experiments were performed in a rapid thermal annealer in an air ambient. The samples were dried at 300 °C for 5 min prior to the isothermal tests. The fraction crystallized is defined as the relative intensity of the (2 1 1) HA diffraction line found in the film after an isothermal anneal compared to the intensity found in fully crystallized material.

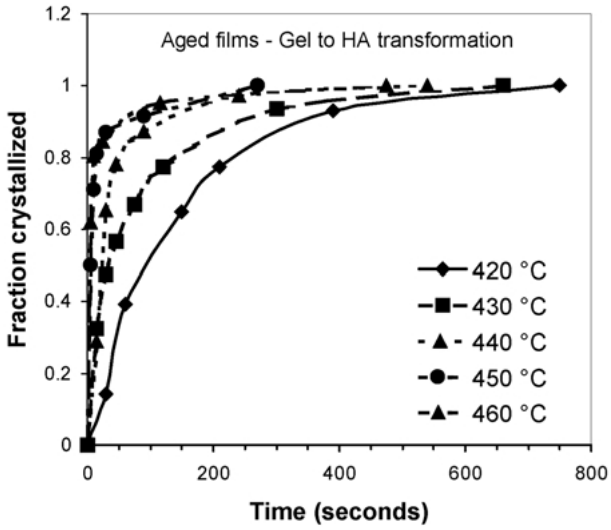

Figure 3 Isothermal growth curves corresponding to the transformation from the amorphous film to crystalline HA in aged films. The experiments were performed in a rapid thermal annealer in an air ambient. The samples were dried at 300 °C for 5 min and then aged at 350 °C for three min prior to the isothermal tests. The fraction crystallized is defined as the relative intensity of the (2 1 1) HA diffraction line found in the film after an isothermal anneal compared to the intensity found in fully crystallized material.

TABLE II Constants for the Avrami relation, $X = 1 - \exp(-\kappa t^n)$, $\kappa = \kappa_0 \exp(-E_a/kT)$

Transformation	Temperature (°C)	n	κ	r	κ_0	E_a (kJ/mol) [eV]
Gel → HA	420	0.55	0.114	0.97		
Gel → HA	435	1.65	0.004	0.99		
Gel → HA	445	0.17	0.94	1.0		
Gel → HA	455	0.28	0.94	0.96		
Average		0.66			4.26×10^{20}	189 [1.96]
Gel → HA, aged	420	1.07	0.005	0.99		
Gel → HA, aged	430	0.64	0.07	0.99		
Gel → HA, aged	440	0.788	0.058	0.95		
Gel → HA, aged	450	0.42	0.44	0.93		
Gel → HA, aged	460	0.34	0.64	0.97		
Average		0.65			1.17×10^{18}	231 [2.39]
HA → TCP	840	1.64	5.5×10^{-5}	0.99		
HA → TCP	860	1.26	1.3×10^{-3}	0.99		
HA → TCP	880	1.67	1.5×10^{-3}	0.97		
HA → TCP	900	1.4	6.7×10^{-3}	0.99		
HA → TCP	920	1.62	5.5×10^{-5}	1.0		
Average		1.52			2.77×10^{16}	492 [5.1]
Gel → TCP	860	1.49	4.2×10^{-4}	0.96		
Gel → TCP	900	1.56	1.2×10^{-3}	1.0		

values of all the intermediate variables are found in Table II.

As a test of the robustness of the activation energy calculation, the activation energy, for the aged samples, was recalculated using a value for the fraction transformed of 0.6 instead of 0.8. The value corresponding to the fraction transformed of 0.6 differed from the value corresponding to 0.8 by 4% (new value = 241 kJ/mol), which is taken as the computational error in the activation energy determination.

The time-temperature transformation diagram was constructed using the isothermal growth curves by choosing a certain fraction transformed, X, and determining, for each temperature, the corresponding time at which that fraction transformed was obtained. A value of $X = 0.8$ was again chosen for this purpose. The resulting *T-T-T* curve is shown in Fig. 5. It is evident that the characteristic ''C'' shape, typically found in transformation studies from a high to low temperature phase, is not observed. An explanation for this behavior can be found in the Discussion section. It can also be seen that the effect of aging is to decrease the rate of crystallization, an effect that becomes less significant at higher temperatures.

Load deflection curves for the aged and unaged samples are shown in Fig. 6. It is evident that the hardness (load/projected area of the indentor) of the aged sample is larger than that of the unaged sample. It is believed that the increased hardness of the aged sample is

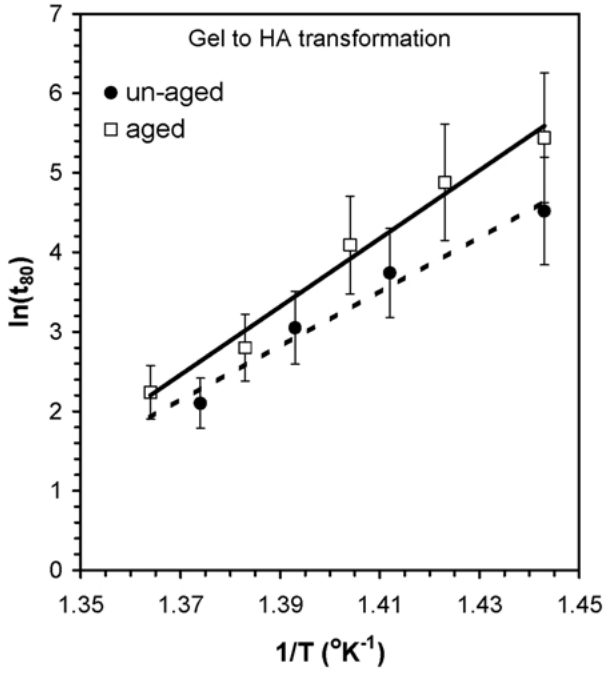

Figure 4 Arrhenius diagram used to determine the activation energy corresponding to the formation and growth of HA from the amorphous film. On the *y*-axis, t_{80} is the time, in seconds, required to obtain 80% relative crystallinity. The data were obtained from the isothermal tests, and it is evident that the data follow linear behavior. The activation energy is found from the slope of the line.

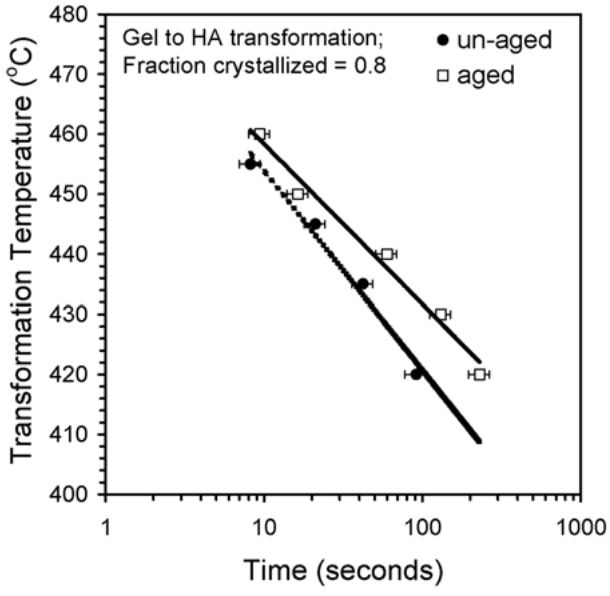

Figure 5 Time-temperature transformation (*T-T-T*) diagram corresponding to the amorphous film to HA transformation in aged and unaged films. The indicated lines correspond to a relative degree of crystallinity of 80%. It can be seen from the upward displacement of the line (and shift to longer times) that the aged sample crystallizes at a lower rate than the unaged sample. This effect is less pronounced as the temperature increases, as indicated by the convergence of the two lines.

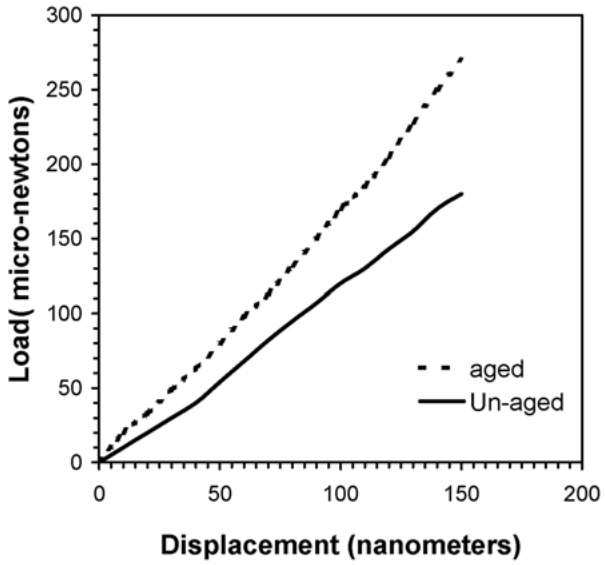

Figure 6 Load-deflection curves of aged and unaged films obtained from nano-indentation. Both films underwent a drying cycle of 300 °C for 5 min; and the aged sample was held an additional 3 min at 350 °C. Both films were approximately 900 nm thick.

due to a greater degree of bonding of the phosphate tetrahedra. Further explanation on this point can be found in the Discussion section.

3.2. HA to TCP transformation

An X-ray spectrum of a sample fired at 750 °C for three minutes (to form a crystalline HA structure), and then at 900 °C for 60 s is shown in Fig. 7. Also shown are the JCPDS standards for α- [18] and β-TCP [19]. It can be seen that the crystalline HA phase has totally transformed into α- and β-TCP. It has been shown that α- and β-TCP can coexist [20, 21]. In light of this, the

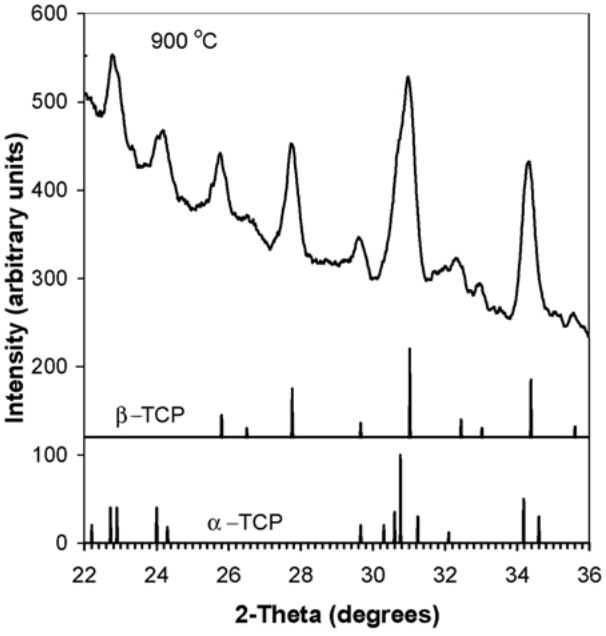

Figure 7 X-ray diffraction pattern of a film first held at 750 °C for 3 min to form a highly crystalline HA structure, and then held at 900 °C for 1 min to form tricalcium phosphate (TCP). Also shown are the JCPDS powder patterns for α-[18] and β-TCP [19]. It can be seen that both of the latter phases are present. $\lambda = 0.15406$ nm.

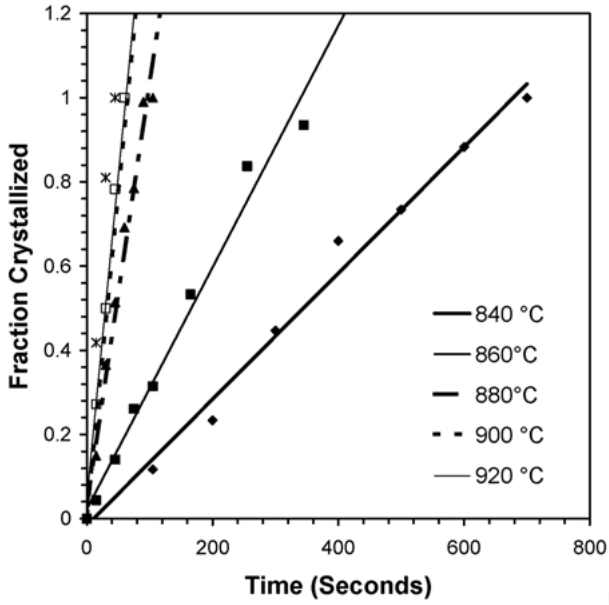

Figure 8 Isothermal growth curves for the formation of β-TCP from HA. The experiments were performed in a rapid thermal annealer in an air ambient. The fraction crystallized is defined as the relative intensity of the (2 1 1) HA diffraction line found in the film after an isothermal anneal compared to the intensity found in fully crystallized material. Linear fits are shown through the data – the values for n and k listed in Table I, however, were obtained from fitting the data to the Avrami equation.

transformation of HA to both α- and β-TCP found here is reasonable. Since the intensity of the β-TCP diffraction line was monitored in the isothermal tests, the results described below strictly apply to the HA to β-TCP transformation.

The results of the isothermal tests corresponding to the HA to β-TCP transformation are shown together with linear fits in Fig. 8. The data correlates well with the Avrami equation as shown in Fig. 8 and as indicated by the correlation coefficients given in Table II. An activation energy of 492 kJ/mol (5.1 eV/atom) was found for this transformation by plotting $\ln(t_{80})$ vs. $1/T$, as shown in Fig. 9 and described above. The *T-T-T* diagram, corresponding to 80% transformation, is shown in Fig. 10. A least squares linear fit is also shown. The *T*-

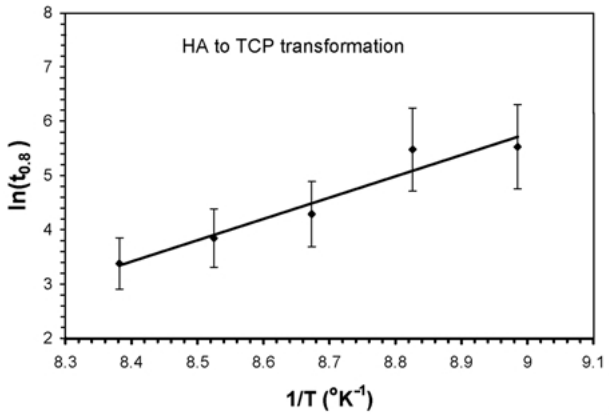

Figure 9 Arrhenius diagram used to determine the activation energy corresponding to the formation and growth of β-TCP from HA. On the y-axis, t_{80} is the time, in seconds, required to obtain 80% relative crystallinity. The data were obtained from the isothermal tests, and it is evident that the data follow linear behavior. The activation energy is found from the slope of the line.

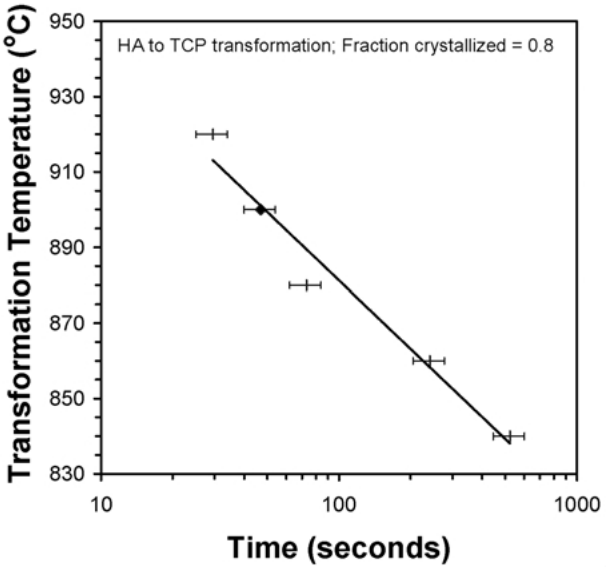

Figure 10 Time-temperature-transformation diagram corresponding to the HA to β-TCP transformation. The indicated line corresponds to a relative degree of crystallinity of 80%.

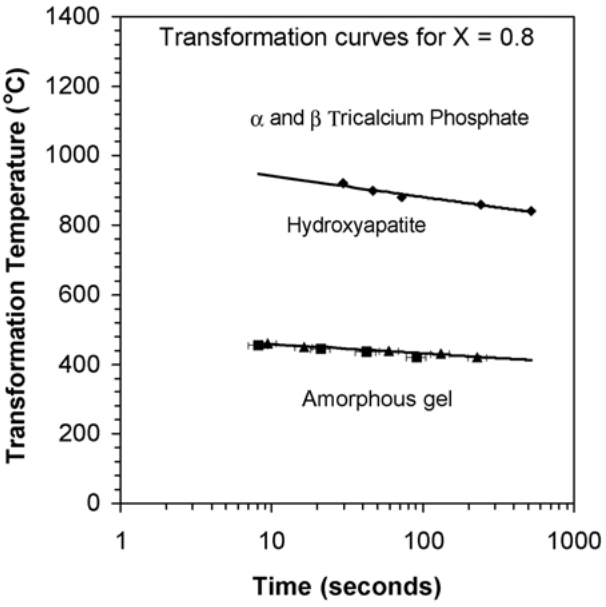

Figure 11 Time-temperature-transformation curves for the amorphous film to crystalline HA and HA to β-TCP transformations.

T-T curves corresponding to the amorphous film to HA and HA to TCP phases are shown in Fig. 11, where it can be seen that at large region exists in which HA is the solitary phase.

4. Discussion

The presumed structure of the dried films (before firing) is that of a condensed phosphate derived from the condensation reaction of H_3PO_4 molecules in the hydrated precursor sol. While studies in other systems have identified amorphous calcium phosphate (ACP) and octacalcium phosphate (OCP) as precursors for HA formation [22], no evidence for these compounds was found in the unfired films. It is believed that the need to break the P—O—P bonds of the condensed phosphate is the reason why elevated temperatures are required to form HA in this system. The activation energy for the breakage of the P—O—P bond ranges from 83.7 to 167.4 kJ/mol [23], and is a function of position of the bond and environmental factors. The fact that the activation energy of this transformation found in this study, 189 kJ/mol, is close to the upper range of the value needed to break P—O—P bonds is an indication that the need to break the P—O—P bonds is the limiting factor to forming HA in this system.

In a study of the transformation of HA from amorphous calcium phosphate (ACP), Layrolle *et al*. determined that the activation energy corresponding to the growth of HA, from an ACP precursor, was 37 kJ/mol, less than 25% of the activation energy found here [24]. As ACP does not contain P—O—P bonds, this result supports the above hypothesis that HA forms readily in a system that does not contain P—O—P bonds.

It should be noted that in another study of the growth of HA from ACP, Gross *et al*. found an activation energy of 274 kJ/mol [25], more than seven times as large as found by Layrolle *et al*. [24]. The reason for the discrepancy between the two groups is not known, but may be due to the different methods used to derive the activation energy.

It was shown in Fig. 5 that the *T-T-T* curve corresponding to the amorphous film to crystalline HA transformation was linear. This result is in agreement with kinetic studies performed on metallic glasses, in which it was shown that the characteristic ''C'' shape of the *T-T-T* curve, corresponding to a maximum value of the crystallization rate, was absent [26, 27]. The ''C'' shape curve of *T-T-T* diagrams, generally seen in the transformation from a liquid to solid phase, is due to the existence of two competing mechanisms: (1) increasing the degree of undercooling $(T_{\text{melt}} - T)$ increases the driving force for crystallization while (2) decreasing the atomic mobility [15]. The combination of these two effects leads to the existence of a temperature at which a maximum rate of crystallization occurs. When kinetic studies are performed on glasses, however, the initial state of the material corresponds to a degree of undercooling very much higher than that found in systems taken from the melt. Hydroxyapatite has a melting temperature of 1550 °C [28], and thus the amount of undercooling at a firing temperature of 450 is 1100 °C. The limiting factor in forming crystalline HA is thus the atomic mobility, and increasing the firing temperature therefore leads to a monotonic increase in the crystallization rate.

It was shown in Fig. 5 that the transformation to HA in the aged films occurred at a lower rate than that in the unaged films, and that the activation energy for the transformation was larger in the aged films. A possible explanation for this results is as follows. It is believed that the aging process, performed below the HA crystallization temperature, causes an increased fraction of PO_4 tetrahedra to bond together, via sharing of a common corner oxygen. Supporting evidence for this increase in degree of bonding is from the fact that it was shown (Fig. 6) that aging increased the hardness of the films. Since it was proposed above that the main barrier to HA crystallization, in this system, is the presence of P—O—P bonds in the amorphous state, an increased number of such bonds would presumably further hinder

formation of crystalline HA. Furthermore, an increase in the strength of gels after room temperature aging has been observed in many systems [29]. In general, the increase in strength is attributed to an increase in the degree of polymerization of the gel network.

As a general statement on the use of Avrami formalism to describe the extent of phase transformations, it should be noted that determination of the value of n does not uniquely determine the mode of transformation. This value depends on the nature of both the nucleation and growth processes [16]. Therefore, a definitive determination of the growth mechanisms requires that the kinetics of at least one of these processes be independently determined. Several strong trends in the values of this constant obtained from this study, however, may be used to distinguish between different mechanisms. The fact that the value of n is identical in the amorphous gel to HA transformation $(n = 0.66)$ for both the aged and unaged samples suggests, for instance, that there is a common mode of transformation. Similarly, the very different value obtained for the HA to TCP transformation $(n = 1.5)$ suggests that a different mechanism is responsible for this reaction. This result is reasonable, since the HA to TCP transformation requires a change of composition between the two phases, from $[Ca/P]_{HA} = 1.667$ to $[Ca/P]_{TCP} = 1.5$. Note that the phase diagram of the $CaO–P_2O_5$ system (dry ambient) indicates that the stable phase of tri-calcium phosphate below 1120 °C is the β form; while above 1120 °C, the α form is stable [22]. It has also been shown that, depending on the method of synthesis, both α and β TCP can be present at temperatures as low as 400 °C [28]. Apparently, the transformation kinetics of β- to α-TCP are very slow at low temperatures, and unstable phases can exist for long times. Also, the value of n for the amorphous gel to TCP transformation is the same as that found in the HA to TCP transformation. It may be inferred from this that crystalline HA is being formed (from the gel) during the first few seconds of heating, and subsequently transforming to TCP.

Densification via viscous flow typically starts at 500 °C in amorphous sol-gel systems, after the completion of the drying stage [3]. The *T-T-T* curves for the amorphous gel to crystalline HA transformation shown in Fig. 5 indicate, however, that the film will crystallize well before viscous flow can start. Viscous sintering is therefore precluded in this system. This result is in agreement with other studies of densification of sol-gel derived HA, in which it was found that little densification occurred below 900 °C [25].

As noted above, TCP has a lower Ca/P ratio than HA and thus a calcium rich phase must form together with TCP. Evidence for the presence of such a phase, calcium oxide (CaO), was indeed found in previous X-ray diffraction studies on powders and thin films synthesized using this method [9, 10].

5. Conclusions

The growth kinetics of crystalline HA and TCP from sol-gel derived thin films have been determined over the temperature range of 420–920 °C. The Avrami formalism was used to describe the rate of crystallization, and it was shown that the mechanism of crystallization differed between the HA and TCP phases. The formation of crystalline HA was found to be very rapid at temperatures above 460 °C, thus precluding the possibility of viscous sintering in this system. It is believed that the barrier to formation of crystalline HA at lower temperatures is the need to break P—O—P bonds in the amorphous, precursor structure.

References

1. J. M. SPIVAK, *J. Biomed. Mat. Res.* **24** (1990) 1121.
2. D. M. LIU, H. M. CHOU and J. D. WU, *J. Mat. Sci. Mat. Med.* **5** (1994) 147.
3. C. J. BRINKER and G. W. SCHERER, in ''Sol-Gel Science'' (Academic Press Inc., Boston, 1990).
4. T. L. ALFORD, S. W. RUSSELL, V. B. PIZZICONI, J. W. MAYER, T. R. LEVINE, M. NASTASI, C. M. COTELL and R. C. AUYEUNG, MRS Proc. **356** (1994).
5. C. M. LOPATIN, T. L. ALFORD, V. B. PIZZICONI, M. KUAN and T. LAURSEN, *Nucl. Inst. Meth. B* **145** (1998) 522.
6. G. W. SCHERER, C. J. BRINKER and E. P. ROTH, *J. Non. Cryst. Sol.* **72** (1985) 369.
7. J. L. KEDDIE and E. P. GIANNELIS, *J. Am. Cer. Soc.* **74** (1991) 2669.
8. L. L. HENCH and D. R. ULRICH, editors, in ''Science of Ceramic Chemical Processing'' (Wiley, N.Y., 1986).
9. C. M. LOPATIN, V. B. PIZZICONI, T. L. ALFORD and T. LAURSEN, *Thin Solid Films* **326** (1998) 227.
10. S. W. RUSSELL, K. A. LUPTAK, C. T. A. SUCHICITAL, T. L. ALFORD and V. B. PIZZICONI, *J. Am. Cer. Soc.* **79** (1996) 837.
11. C. M. LOPATIN, T. L. ALFORD, V. B. PIZZICONI and T. LAURSEN, *Materials Letters* **37** (1998) 211.
12. Z. CONGHAN, J. PHALIPPOU and J. ZARZYCKI, *J. Non. Crys. Sol.* **82** (1998) 321.
13. JCPDS Card No. 9–432, 1994.
14. T. KANAZAWA, in ''Inorganic Phosphate Materials'' (Kodansha, Tokyo, 1989) p. 82.
15. D. A. PORTER and K. E. EASTERLING, in ''Phase Transformations in Metals and Alloys'' (Chapman & Hall, London, 1992) p. 290.
16. J. W. CHRISTIAN, in ''The Theory of Transformations in Metals and Alloys'' (Pergamon, Oxford, 1975).
17. K. N. TU, J. W. MAYER and L. C. FELDMAN, in ''Electronic Thin Film Science'' (McMillan Pub. Co., N.Y., 1992) p. 262.
18. JCPDS Card No. 9–342, 1994.
19. JCPDS Card No. 9–169, 1994.
20. T. KANAZAWA, in ''Inorganic Phosphate Materials'' (Kodansha, Tokyo, 1989) p. 80.
21. E. D. EANES, *Calc. Tiss. Res.* **5** (1970) 133.
22. T. KANAZAWA, in ''Inorganic Phosphate Materials'' (Kodansha, Tokyo, 1989) p. 85.
23. R. VAN WAZER, in ''Phosphorus and Its Compounds'' (Interscience Publishers, Inc. N.Y., 1958) p. 515.
24. P. LAYROLLE, A. ITO and T. TETEISHI, *J. Am. Cer. Soc.* **81** (1998) 1421.
25. K. A. GROSS, V. GROSS and C. C. BERNDT, *J. Am. Cer. Soc.* **81** (1998) 106.
26. S. SURINACH, M. D. BARO, J. A. DIEGO, N. CLAVAGUERA and M. T. CLAVAGUERA-MORA, *Acta Metall. Mater.* **40** (1992) 37.
27. H. Y. TONG, B. Z. DING, J. G. JIANG, K. LU, T. WANG and Z. Q. HU, *J. Appl. Phys.* **75** (1994) 654.
28. T. YAMAMURO, L. L. HENCH and J. WILSON, editors, in ''Handbook of Bioactive Ceramics'', V. II (CRC Press, Boston, 1990) p. 8.
29. C. J. BRINKER and G. W. SCHERER, in ''Sol-Gel Science'' (Academic Press Inc., Boston, 1990) p. 390.

Received 17 October
and accepted 26 December 2000